AD-A284 029

ICASE

LINEAR BICHARACTERISTIC SCHEMES WITHOUT DISSIPATION

DTIC
ELECTED
SEP 0 8 1994
F

Philip Roe

94-29068

DTIC QUALITY INSPECTED 3

USRA Operated by Universities Space Research Association

94 9 06 113

Linear Bicharacteristic Schemes Without Dissipation

Philip Roe*
W.M. Keck Foundation
Laboratory for Computational Fluid Dynamics
Department of Aerospace Engineering
University of Michigan
Ann Arbor, MI 48109-2140

Abstract

This paper is concerned with developing methods for the propagation of linear waves in several space dimensions. The methods are time-reversible, and hence free from numerical dissipation. They are based on bicharacteristic forms of the governing equations, and are made possible by adopting forms of staggered storage that depend on the precise equations under consideration. Analysis is presented for the equations of acoustics, electromagnetics, and elastodynamics.

Accesion For

NTIS	CRA&I	☑
DTIC	TAB	☐
Unannounced		☐
Justification		

By ....

Distribution /

Availability ....

Dist	Avail and / or Special

A-1

1 Introduction

In Computational Physics we solve numerically some discrete replacement of the governing equations, often because those equations are nonlinear, and hence not amenable to analytical treatment. There is a comparative neglect of linear problems, except as preliminary models on which to illustrate algorithmic principles. There are however many linear problems that are technically important in their own right, and which demand huge computational resources, due to the neccessity of representing very complicated solutions. In this paper we shall be concerned with problems in which low amplitude wave propagation takes place over distances typified by large multiples of the wavelength. A few of the areas and applications where such problems arise are

1. Acoustics and Aeroacoustics, for noise abatement

2. Electromagnetics, for microcircuit design,

3. Elastodynamics, for nondestructive testing,

4. Seismology, for oil exploration,

5. Medical Imaging, for accurate diagnosis,

6. Hyperthermia, for noninvasive surgery.

In some of these cases, the wavelengthss are required to be small compared to the obstacles they travel round, to enable accurate measurements, but if the wavelengths are not so small that geometrical optics can be applied, we have an 'intermediate regime' that is computationally the most demanding. In other cases, this regime arises by accident rather than design. Either way, there is a need to propagate small-amplitude waves over tens or hundreds of wavelengths with minimal dispersion and damping.

The view taken here will be that, although both kinds of error are important, it is often damping that is the more damaging to practical calculations. A wave that is excessively damped simply disappears, and there is no solution to see. Dispersion leaves the wave intact, but in the wrong place. If all waves were to propagate at the same wrong speed, we would have a good answer to a question that differs from the one intended; our waves would propagate in the wrong medium. However, since the data we have concerning that medium is usually inexact, this may not be of great concern. In this paper, we consider schemes that by construction are completely free from dissipation and which maintain dispersion errors within some acceptable limits.

The schemes studied here are leapfrog methods (which are inherently free of dissipation) but combined with upwind bias. Such schemes were first described by Iserles[1] for one-dimensional advection. Compared with classical leapfrog methods they have more compact stencils, leading to improved accuracy and more natural handling of boundaries. An account of the one-dimensional methods is provided in Section 2, which provides a summary, commentary, and extension of [1].

The present paper gives the first use of these methods in higher dimensions, and the generalisation involves some new ideas. For any characteristic-based scheme there is a need to reconcile computational convenience and physical motivation. These issues are discussed in Section 3. In Section 4 it is shown that one solution is to introduce staggered storage, in a manner dictated by the coupling of unknowns in the given equation set. Particular examples discussed are the equations of acoustics, elastodynamics, and electromagnetics. Computational results are presented in Section 5.
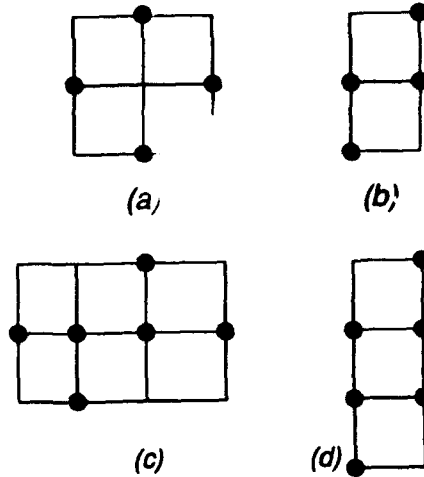
Figure 1: Four symmetric stencils for wave propagation. (a) classical leapfrog, (b) Upwind leapfrog, (c) Upwind leapfrog extended in space, (d) Upwind leapfrog extended in time.

2 Upwind Leapfrog Schemes in One Dimension

2.1 Symmetry and Dissipation

To solve any wave propagation problem without introducing dissipation, it is obviously necessary that the scheme employed be reversible in time. This implies that the stencil on which the scheme is supported has central symmetry, as is the case for the four stencils shown in Figure 1. Example (a) is the stencil for the classical leapfrog scheme. This has symmetry both in space (left-right) and in time (forward-backward). However, the weaker (point) symmetry of the other examples is also adequate to ensure reversibility. A scheme without dissipation can be used to integrate from given data at $t = 0$ to a solution at $t = T$, and then, with time reversed, integrated back to $t = 0$ to recover the data exactly (apart from roundoff errors). During the reverse integration the direction of wave propagation is also reversed; hence the requirement is for the stencil to remain invariant under a 180° rotation.

It is also neccessary for reversibility that the coefficients of the scheme be symmetrical. If the scheme, for some scalar problem in which the unknown is u is written

$$\sum c_p u_p = 0$$

then the condition

$$c_{p1} + c_{p2} = 0$$

where $p1, p2$ are any pair of points that exchange places under the rotation, is neccessary and sufficient to ensure reversibility.

The modified equation of such a scheme contains no even order derivatives; as an approximation to a first-order PDE it therefore has even order of accuracy.

2.2 Errors and Stability Bounds

2.2.1 Stencil 1a

On the stencil of Figure 1(a) the only consistent scheme for linear advection

$$u_t + a u_x = 0$$

is the regular leapfrog method

$$u_j^{n+1} = u_j^{n-1} - \nu \left(u_{j+1}^n - u_{j-1}^n \right) \tag{1}$$

where the Courant number $\nu = a \Delta t / \Delta x$.

For this and other reversible methods the dispersion relationship can be found by assuming solutions of the form

$$u_j^n = \exp i(n\phi - j\theta) \tag{2}$$

Given a real value for the Fourier angle θ, finding a real value for the phase change ϕ will indicate that the method is dissipationless as assumed. A complex value of ϕ means that $\exp i\phi$ is not on the unit circle, and hence that there are amplification factors a_1, a_2 exhibiting growth or decay. Time reversibility implies that $a_1 a_2 = 1$, and so the scheme has an unstable mode in either direction.

Substituting (2) into (1) gives the dispersion relationship as

$$\sin \phi = \nu \sin \theta$$

and it is evident that the scheme is unstable for some θ if $\nu > 1$.

For $\nu < 1$ the only error is in phase speed. A signal such as (2) travels with speed

$$a_N = \frac{\phi}{\theta} \frac{\Delta x}{\Delta t}$$

We therefore define the phase speed error as

$$
\begin{aligned}
\varepsilon_p &= \frac{\frac{\phi}{\theta}\frac{\Delta x}{\Delta t} - a}{\frac{\Delta x}{\Delta t}} \\
&= \frac{\phi}{\theta} - \nu \tag{3} \\
&\simeq \frac{\theta^2}{6}\nu(\nu^2 - 1) \tag{4}
\end{aligned}
$$

Here the 'grid speed' $\Delta x/\Delta t$ has been used to make the error non-dimensional. To achieve a target accuracy of 1% in this measure the regular leapfrog scheme requires typically 15 mesh points to resolve one wavelength, and about 45 to meet the more stringent target of 0.1%. This criterion of N points per wavelength will be used frequently in what follows to measure the resolving power of an algorithm. Note that $N = 2\pi/\theta$.

2.2.2 Stencil 1b

The stencil in Figure 1(b) leads to a scheme that is the simplest member of the class considered by Iserles [1]. On this stencil u_t is approximated using the average evaluated

over the two time-like legs, and u_x using the single space-like leg. After collecting terms, we obtain the scheme

$$u_{j+1}^{n+1} - u_j^{n-1} = (1 - 2\nu) \left(u_{j+1}^n - u_j^n \right).$$ (5)

The dispersion relationship for this scheme is

$$\sin\left(\phi - \theta/2\right) + (1 - 2\nu)\sin\theta/2 = 0.$$

For stability, we see that we must have

$$-1 \leq 1 - 2\nu \leq 1,$$

implying $0 \leq \nu \leq 1$. [1] This stencil, as we might have guessed, is appropriate only for right-going waves. For left-going waves the mirror image of this stencil is needed.

The leading term of the phase error is

$$\varepsilon_p \simeq \frac{\theta^2}{12}\nu(1 - \nu)(1 - 2\nu)$$

Target errors of 1.0% or 0.1%, are met for all ν by a resolution of $N \geq 6$ or $N \geq 18$ respectively. This scheme is roughly three times as economical as regular leapfrog.

2.2.3 Stencil 1c

Further improvements are possible by creating higher-order schemes. On the stencil of Figure 1(c) the time derivative can be approximated as previously, but the space derivative may have weight k given to the inner interval and weights $\frac{1}{2}(1 - k)$ to each outer interval. The resulting scheme is

$$u_{j+1}^{n+1} - u_j^{n-1} = (1 + \nu(1 - 3k)) \left(u_{j+1}^n - u_j^n \right) + \nu(1 - k) \left(u_{j+2}^n - u_{j-1}^n \right),$$ (6)

with dispersion relationship

$$\sin\left(\phi - \theta/2\right) + (1 + \nu(1 - 3k))\sin\theta/2 - \nu(1 - k)\sin 3\theta/2 = 0$$

This scheme has a leading phase error of

$$\varepsilon_p = \frac{\nu\theta^2}{6} \left[\nu^2 - \frac{3\nu}{2} - \frac{5}{4} + \frac{3k}{2} \right].$$

If this is eliminated by choosing

$$k = \frac{5 + 6\nu - 4\nu^2}{6}$$

we obtain the scheme

$$u_{j+1}^{n+1} - u_j^{n-1} = -\frac{1}{2}(1+\nu)(2-\nu)(1-2\nu) \left(u_{j+1}^n - u_j^n \right) + \frac{1}{6}\nu(1-\nu)(1-2\nu) \left(u_{j+2}^n - u_{j-1}^n \right),$$ (7)

which was also noted by Iserles. The dispersion relationship can be arranged to read

$$\sin\left(\phi - \theta/2\right) = (2\nu - 1)\sin\theta/2 \left[1 + \frac{2}{3}\nu(1 - \nu)\sin^2\theta/2. \right]$$

---

[1] Iserles gives the stability limit as $0 \leq \nu \leq \frac{1}{2}$ since his stability definition encounters a technical objection when $\nu = \frac{1}{2}$. But since the scheme reduces in that case to $u_{j+1}^{n+1} = u_j^{n-1}$ the objection is insubstantial.

Stability requires that the RHS remains in the interval $[-1, 1]$ and it is clear that this will be so for $0 \leq \nu \leq 1$.

The phase error of this scheme has the leading term

$$\varepsilon_p = \frac{\theta^4}{120} \nu (1 - \nu^2)(1 - 2\nu)(2 - \nu)$$

The target accuracies of 1.0% and 0.1% are achieved by taking $N \geq 4$ and $N \geq 6$ respectively.

2.2.4   Stencil 1d

A different way to achieve fourth-order accuracy is to adopt the stencil of Figure 1(d). Here the two alternative evaluations of u_x must be given equal weight, but the two evaluations of u_t from the middle of the stencil can be given weight $\frac{1}{2}k$, while the evaluations from the upper and lower legs each have weight $\frac{1}{2}(1 - k)$. This leads to the scheme

$$(1 - k) \left(u_{j+1}^{n+1} - u_j^{n-2} \right) = (1 - \nu - 2k) \left(u_{j+1}^n - u_j^{n-1} \right) + (\nu - k) \left(u_j^n - u_{j+1}^{n-1} \right). \qquad (8)$$

The dispersion relationship can be written

$$(1 - k) \sin \frac{3\phi - \theta}{2} + (2k + \nu - 1) \sin \frac{\phi - \theta}{2} - (\nu - k) \sin \frac{\phi + \theta}{2} = 0.$$

The leading error term is

$$\frac{2\theta^2}{3} \nu (1 - \nu) [5\nu - 1 - 6k\nu].$$

After removing this by the choice

$$k = \frac{5\nu - 1}{6\nu}$$

the scheme becomes

$$(1 + \nu) \left(u_{j+1}^{n+1} - u_j^{n-2} \right) = 2(1 + \nu)(1 - 3\nu) \left(u_{j+1}^n - u_j^{n-1} \right) + (1 - 3\nu)(1 - 2\nu) \left(u_j^n - u_{j+1}^{n-1} \right). \qquad (9)$$

and the dispersion relationship becomes

$$(1 + \nu) \sin \frac{3\phi - \theta}{2} - 2(1 + \nu)(1 - 3\nu) \sin \frac{\phi - \theta}{2} - (1 - 3\nu)(1 - 2\nu) \sin \frac{\phi + \theta}{2}. \qquad (10)$$

The leading error term is then

$$\frac{\theta^4}{120} \nu^2 (1 - \nu^2)(1 - 3\nu)(1 - 2\nu).$$

In this case, the target of 1.0% error is met even by $N = 2$, and to achieve 0.1% requires merely $N \geq 3$.

To investigate stability, the dispersion relation (10) can be rearranged as

$$\tan \theta / 2 = \tan \phi / 2 \frac{3\nu - (1 - 2\nu) \tan^2 \phi / 2}{3\nu^2 - (1 + \nu - 3\nu^2) \tan^2 \phi / 2}$$

For any real value of $\tan \theta / 2$, stability requires three real values of $\tan \phi / 2$ (otherwise, as discussed above, one of the two complex roots is unstable). By considering the graph of the expression on the RHS, it is easy to show that three real roots are found if and only if the singularities in the function interlace with its zeros. This implies the stabilty bound $0 \leq \nu \leq \frac{1}{2}$.

2.3 Phase Error Diagrams

For the four schemes discussed above, Figure 2.3 shows the phase error as defined in (4). The improvement at each stage is striking.

2.4 Interpolation Properties of Stencils

For linear advection, all of the above schemes could be derived by using the fact that the solution is constant along characteristics $dx/dt = a$. Referring to Figure 3, the black circles denote places where the data is available, and the open circles places where it can found by extrapolating along a characteristic. A polynomial can be fitted to this combination of values, and an interpolated value can be read off at the open square. This value can then be extrapolated to the black square, where the solution is required. The whole process can be thought of as maximum-order polynomial interpolation in the coordinate $x - at$. It is illuminating to compare the stencils on the left with those on the right. In the latter, the data within which interpolation must be carried out are much more compactly located. This is the basic reason for the improvement in going from (a) to (b) and from (c) to (d).

For problems without constant coefficients, the interpretation will not be so simple, but the advantages of the compact stencil will remain. A desire to group the stencil tightly around the characteristic will lead to upwind biassing.

2.5 Group Velocity and Boundary Procedures.

When waves propagate without dissipation, the concept of group velocity applies. This can be variously interpreted as the speed of a wave packet, or the speed with which energy propagates. Linear first-order PDEs, without source terms, are not dispersive, and so their group velocity is the same as their phase speed. Trefethen [2] has drawn attention to the importance of group velocity for discretized PDEs, which are dispersive. In particular, if the group velocity should have the opposite sign from the phase velocity at any wavenumber, such waves are prone to be introduced into the solution as spurious oscillations by numerical boundary conditions.

Iserles [1] gave two interesting theorems relating to generalised leapfrog schemes with three time levels. The first of these states that if the scheme is to be stable for small Courant numbers, the gap between the two time-like legs must comprise either zero, one, or two space intervals. He then proved that with zero or two intervals, the group velocity would always be in the wrong direction for the shortest waves with $\theta = \pi$. It has the correct sign for stencils with one interval.

The group velocity is defined by

$$a_g = \frac{d\phi}{d\theta} \frac{\Delta x}{\Delta t}$$ (11)

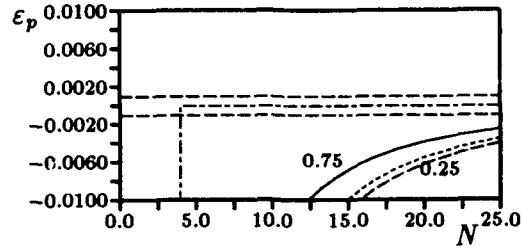Computing this expression for $\theta = \pi$ in each of the four cases yields

6

Figure 2: (a) Phase error as function of resolution for the regular Leapfrog scheme. The dashed horizontal lines correspond to one part per thousand.
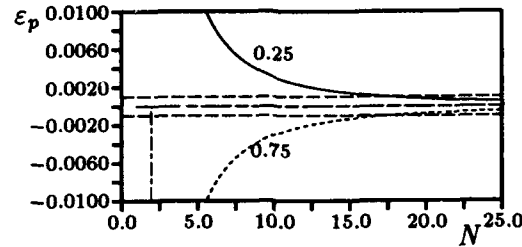

Figure 2: (b) Phase error as function of resolution for the Upwind Leapfrog scheme.
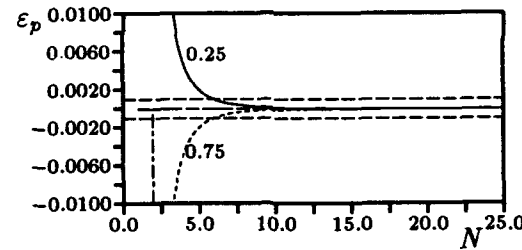

Figure 2: (c) Phase error as function of resolution for the Upwind Leapfrog scheme extended in space.
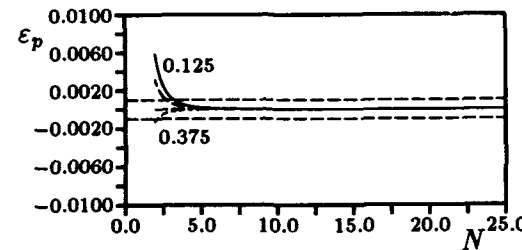

Figure 2: (d) Phase error as function of resolution for the Upwind Leapfrog scheme extended in time. Note that the Courant numbers have been halved.
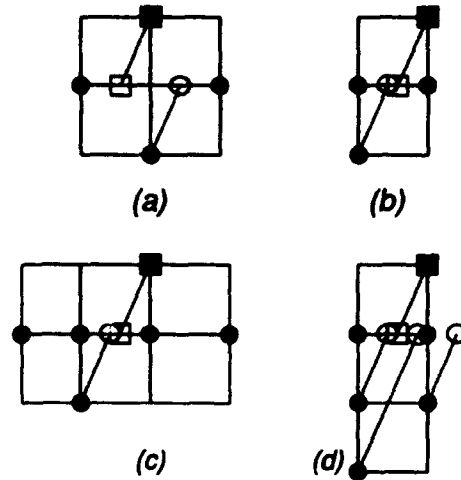
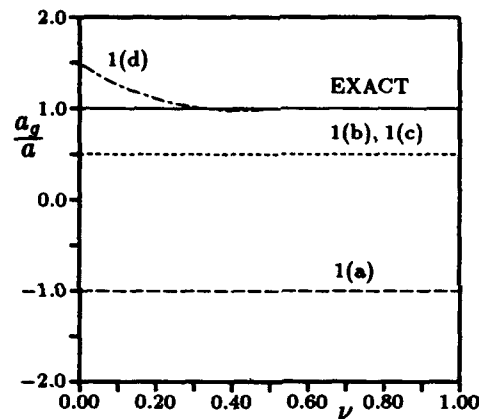Figure 3: Interpretation of the schemes as interpolation schemes

Figure 4: Group velocities of the four schemes for short waves.

Scheme	$\frac{a_g}{a}$
Regular Leapfrog	-1
Upwind Leapfrog	$\frac{1}{2}$
Stencil 1(c)	$\frac{1}{2}$
Stencil 1(d)	$\dfrac{3(1-\nu)}{2(1+\nu-3\nu^2)}$

Figure 2.5 shows these short wave group velocities as functions of Courant number. Cases (a), (b), and (c) exemplify Iserles' theorem. Case (d), which is not covered by the theorem, does best of all, the group velocity being exact when $\nu = \frac{1}{2}, \frac{1}{3}$. Probably the exact value does not matter, since the schemes should not be used to model waves that are so underresolved, but all three of the upwind leapfrog schemes display behaviour that leads to no great anxiety regarding boundary problems.

8

2.6 Second (Spurious) Solutions

A well-known danger of using multi-level schemes is that the dispersion relationship has spurious branches. Here, in the case of stencils (a),(b), or (c), if the phase angles (θ, ϕ) yield a solution, then so do the angles $(\theta, \phi + \pi)$. One of these solutions provides a reasonable approximation to the continuous problem; the other does not. For given θ, the amplification factors of the two solutions are in the ratio

$$\frac{\exp i(\phi + \pi)}{\exp i(\phi)} = -1$$

so that the second solution can be expected to oscillate in time. Such a solution can enter the calculation either if (a) a poor starting procedure is used at the first time-step, or (b) through aliasing caused by nonlinearity, or (c) through the boundary procedures. However, in no calculation made to date with the upwind leapfrog schemes has any contamination occured from these sources.

What have been observed are spurious solutions due to source terms. This danger can easily be demonstrated on the model problem

$$u_t + a u_x = s u \tag{12}$$

whose exact solution is $u(x, t) = e^{st} u(x - at, 0)$. A naive extension of (5) would be

$$u_{j+1}^{n+1} - u_j^{n-1} = (1 - 2\nu) \left(u_{j+1}^n - u_j^n \right) + s \Delta t (u_j + u_{j+1}). \tag{13}$$

The ansatz $u_j^n = g^n \exp ij\theta$ leads to a quadratic equation for the amplification factor g, with roots $g_{1,2}$ whose product is given by

$$g_1 g_2 = \frac{C_j^{n-1}}{C_{j+1}^{n+1}} = 1$$

where C_j^n is the coefficient of u_j^n in the difference scheme. Let g_1 be the amplification factor of the true solution, and g_2 that of the spurious solution. Suppose that $s < 0$, so that the true solution decays. Then $g_1 < 1$, but $g_2 > 1$, and the spurious solution will grow. Even though the mechanism for introducing it may be very weak, it will eventually dominate the calculation.

A way to remove the spurious solution from the model problem is to eliminate the source term by making the substitution

$$u = e^{st} v \quad \Rightarrow \quad v_t + a v_x = 0$$

(Note that this still works if s depends on x, and even if u is a vector and s a matrix.) Now solve for v using (5) and then translate back to u. The result is

$$e^{-s\Delta t} u_{j+1}^{n+1} - e^{s\Delta t} u_j^{n-1} = (1 - 2\nu) \left(u_{j+1}^n - u_j^n \right). \tag{14}$$

By construction, both roots now have the same amplification factor (which is exact), and the spurious root can never come to dominate. Equation (14) can be rearranged to show the source term more explicitly as

$$\begin{aligned} e^{-s\Delta t}(u_{j+1}^{n+1} - u_{j+1}^n) \\ + e^{s\Delta t}(u_j^n - u_j^{n-1}) \end{aligned} = \begin{aligned} -2\nu(u_{j+1}^n - u_j^n) \\ +(1 - e^{-s\Delta t})u_{j+1}^n - (1 - e^{s\Delta t})u_j^n \end{aligned} \tag{15}$$

9

In this form, precise and elaborate instructions appear for evaluating both the time derivative and the source term. However, the far simpler scheme in which $e^{\pm s\Delta t}$ is replaced by $1 \pm s\Delta t$ also has the property that $|g_1| = |g_2|$, in fact

$$|g_1| = |g_2| = \sqrt{\frac{1 + s\Delta t}{1 - s\Delta t}},$$

which approximates $e^{s\Delta t}$ to second order. This provides a practical algorithm in which the spurious solution is always kept under control, provided $s\Delta t$ is not large.

2.7 General Remarks

The Upwind Leapfrog methods have a number of attractive features as starting points for the construction of practical wave propagation algorithms. Chief among these is the fact that clustering the stencil around the characteristic enables high accuracy to be achieved with a low operation count in a fully discrete way. For application to a system of equations the left- and right-going characteristic equations must be discretised on different stencils. The overhead for doing this is the cost of one simple Riemann solution per pair of adjacent points. The second-order Upwind Leapfrog method has been applied in this way to the linear, but non-constant-coefficient problem that arises from placing a noise source in a quasi-one-dimensional nozzle [3]. The version described there was later found to suffer long-time instability due to the second solution discussed above, but the modification described has allowed very long-time calculations to be made (Choolwan Kim, private communication).

Upwinding normally pays dividends at boundaries. Especially as regards Schemes (b) and (d), the use of a two-point stencil in space means that no special procedures are called for at inflow or outflow boundaries. Scheme (c) should be simpler in this regard than other fourth-order methods. Another, related, benefit is the ability to handle locally refined meshes without generating reflected waves.

Multilevel methods require special starting procedures for the first few time steps. For initial-value problems a conventional high-order scheme can be used, but if the solution is excited from the boundaries, as with many wave propagation problems, no problem arises.

All of the methods are conservative, in the sense that for a scheme with l levels

$$\sum_j u_j^{n+l-1} = \sum_j u_j^n + \text{boundary terms.}$$

because all terms at intermediate time levels ' telescope'. If a conservative starting scheme is employed, or if all perturbations originate at the boundary, the schemes are conservative in the conventional sense. However, without a limiting procedure, they cannot be used for nonlinear problems where shocks may form.

Scheme (d) is not suitable for steady-state problems, because its stencil is not broad enough to give better than second-order accuracy in space. However, for wave propagation it keeps its formal accuracy even when ν is vanishingly small.

It is worth noting that for stencils (b) and (d), the order of accuracy is unaffected by any mesh nonuniformity, since only one mesh interval is involved. Of course regular timesteps must be taken.

These considerations provide strong motivation for attempting the extension to higher dimensions, which will be the topic of the remaining sections.
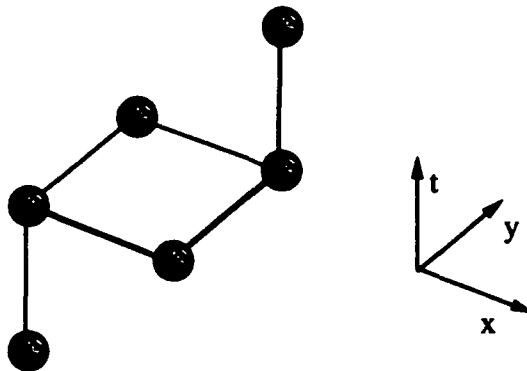
10

Figure 5: Possible stencil for linear advection in two dimensions.

3 Two-dimensional Problems

The natural way to extend upwind leapfrog schemes to advection in two dimensions turns out not to be very fruitful. Consider the stencil in Figure 5. This appears to offer a suitable basis for solving

$$u_t + a u_x + b u_y = 0$$

if $a, b \geq 0$. There is a unique reversible discretization on this stencil that is indeed second-order accurate, and also stable provided $a\Delta t/\Delta x$, $b\Delta t/\Delta y \in [0, 1]$. However, the scheme is dificult to apply in situations in which a, b are not constant. For example, suppose that b is small and frequently changes sign, thereby switching the stencil between two alternatives; if there is a significant curvature in the y-direction this will make for erratic results.

Paradoxically, though, it has proved possible to adapt the upwind leapfrog schemes for sets of coupled wave equations in more than one dimension. A stencil like that in Figure 5 is used to discretise a bicharacteristic form of the equations. Because the chosen bicharacteristics are related to the grid rather than the solution, no switching occurs.

The presentation will concentrate on generalisations of the scheme defined by stencil 1b. Generalisation of the regular leapfrog scheme (stencil 1a) of course presents no problems. A generalisation of the fourth-order scheme defined by stencil 1c is possible, and forms part of the thesis work of my student J. P. Thomas. At present it appears difficult to generalise the scheme defined by stencil 1d.

Before presenting the actual discretisation, however, it is neccessary to make some remarks on the general subject of bicharacteristic equations and their discrete versions.

3.1 Bicharacteristic Equations

Consider a hyperbolic set of partial differential equations in D space dimensions plus time $(x_1, x_2, \cdots, x_D; t)$, written as

$$\frac{\partial \mathbf{u}}{\partial t} + \sum_{d=1}^{d=D} A_d \frac{\partial \mathbf{u}}{\partial x_d} = 0 \qquad (16)$$

Premultiply this equation by $\mathbf{l}_1$, a left eigenvector of A_1 having eigenvalue λ_1. This involves no loss of generality, since we can always rotate the coordinates to align x_1 with any required

direction. The result is

$$\left(\frac{\partial}{\partial t} + \lambda_1 \frac{\partial}{\partial x_1}\right) l_1 u + \sum_{d=2}^{d=D} l_1 A_d \frac{\partial u}{\partial x_d}. \tag{17}$$

This is called a *characteristic equation*. The number of independent variables has been reduced by one compared with the original form. The characteristic equation holds in a D-dimensional subset, or manifold, of the $D + 1$-dimensional space-time. Derivatives normal to this manifold do not appear in this equation. They are allowed to be discontinuous across the manifold, which is thereby identified as a wavefront. Reduction of the dimension by more than one is not possible unless an l can be found that is a left eigenvector for more than one A.

Special significance is often given to writing the characteristic equation in a particular form. Derivatives within the characteristic manifold can be written along any convenient set of geometric basis vectors. One element of the basis set can be chosen as the intersection of the characteristic manifold with a neighbouring characteristic manifold. The characteristic equation then has the appearance of an ordinary differential equation along that intersection, together with "source terms", and is called a *bicharacteristic equation*.

Numerical methods based on characteristic or bicharacteristic equations have often been proposed in the literature. Good surveys of early work can be found in the survey paper of Chuskin [3] and the thesis of Camarero[4]. More recent work has been done by [5,6]. However, the clear connection between physical interpretation, differencing techniques and solution quality that is found for one-dimensional problems has remained largely elusive. The methods work, but show no striking advantage. Reasons for this will be discussed later, but we next give two examples of problems formulated as (bi)characteristic equations. Only the two-dimensional case is presented, but the extension to three is natural.

3.2 Acoustic Waves

The governing equations for acoustic waves in a uniform medium can be written in the form (2) with unknowns $u = (u, v, p)^T$ corresponding to two velocity components and pressure. The matrices are

$$A_1 = \begin{vmatrix} 0 & 0 & 1/\rho \\ 0 & 0 & 0 \\ \rho a^2 & 0 & 0 \end{vmatrix}, \quad A_2 = \begin{vmatrix} 0 & 0 & 0 \\ 0 & 0 & 1/\rho \\ 0 & \rho a^2 & 0 \end{vmatrix}, \tag{18}$$

where ρ is the density of the medium, and a the sound speed. The eigenvalues of A_1 are $\lambda = \pm a, 0$. The eigenvector corresponding to $\lambda = 0$ does not yield an interesting result, but the other left eigenvectors are $(\rho a, 0, \pm 1)$ giving the characteristic equations

$$\frac{\partial p}{\partial t} + a\frac{\partial p}{\partial x} + \rho a \left(\frac{\partial u}{\partial t} + a\frac{\partial u}{\partial x}\right) = -\rho a^2 \frac{\partial v}{\partial y} \tag{19}$$

$$\frac{\partial p}{\partial t} - a\frac{\partial p}{\partial x} - \rho a \left(\frac{\partial u}{\partial t} - a\frac{\partial u}{\partial x}\right) = -\rho a^2 \frac{\partial v}{\partial y} \tag{20}$$

These are the characteristic equations for plane waves travelling in the $\pm x$-directions. In this case, they are also the bicharacteristic equations. The bicharacteristic equations for waves travelling in the $\pm y$-directions are

$$\frac{\partial p}{\partial t} + a\frac{\partial p}{\partial y} + \rho a \left(\frac{\partial v}{\partial t} + a\frac{\partial v}{\partial y}\right) = -\rho a^2 \frac{\partial u}{\partial x} \tag{21}$$

12

$$\frac{\partial p}{\partial t} - a\frac{\partial p}{\partial y} - \rho a\left(\frac{\partial v}{\partial t} - a\frac{\partial v}{\partial y}\right) = -\rho a^2\frac{\partial u}{\partial x} \tag{22}$$

For an arbitrary direction of travel the result is found through multiplication by $(\rho a\cos\theta, \rho a\sin\theta, 1)$.

3.3 Elastodynamic Waves

Consider an isotropic elastic medium undergoing small transient displacements. To apply the characteristic analysis the governing equations must be written as a first-order system. There are many ways to do this, according to the choice of dependent variables. Here we choose $\mathbf{u} = (u, v, p, q, \tau)$ where again u, v are velocities, p, q are the normal stresses on surfaces of constant x, y, and τ is the shear stress. For this problem we have

$$A_1 = -\begin{vmatrix} 0 & 0 & 1/\rho & 0 & 0 \\ 0 & 0 & 0 & 0 & 1/\rho \\ \rho c_1^2 & 0 & 0 & 0 & 0 \\ \alpha\rho c_1^2 & 0 & 0 & 0 & 0 \\ 0 & \rho c_2^2 & 0 & 0 & 0 \end{vmatrix}, \quad A_2 = -\begin{vmatrix} 0 & 0 & 0 & 0 & 1/\rho \\ 0 & 0 & 0 & 1/\rho & 0 \\ 0 & \alpha\rho c_1^2 & 0 & 0 & 0 \\ 0 & \rho c_1^2 & 0 & 0 & 0 \\ \rho c_2^2 & 0 & 0 & 0 & 0 \end{vmatrix}, \tag{23}$$

Here, c_1 is the speed of propagation for longitudinal waves, which bring about irrotational displacements, and c_2 is the propagation speed for transverse waves, which produce divergence-free dispacements. The parameter α is defined by $\alpha = 1 - 2(c_2/c_1)^2$, and is about $1/3$ for most metals.

The eigenvalues of A_1 are $(\pm c_1, \pm c_2, 0)$. Again the zero value does not give an interesting result; the remaining left eigenvectors are $(\rho c_1, 0, \pm 1, 0, 0)$ and $(0, \rho c_2, 0, 0, \pm 1)$. The bicharacteristic equations for waves propagating in the $\pm x$-directions are

$$\frac{\partial p}{\partial t} + c_1\frac{\partial p}{\partial x} - \rho c_1\left(\frac{\partial u}{\partial t} + c_1\frac{\partial u}{\partial x}\right) = \alpha\rho c_1^2\frac{\partial v}{\partial y} - c_1\frac{\partial \tau}{\partial y} \tag{24}$$

$$\frac{\partial p}{\partial t} - c_1\frac{\partial p}{\partial x} + \rho c_1\left(\frac{\partial u}{\partial t} - c_1\frac{\partial u}{\partial x}\right) = \alpha\rho c_1^2\frac{\partial v}{\partial y} + c_1\frac{\partial \tau}{\partial y} \tag{25}$$

which relate to the longitudinal waves, which are also called primary waves or P-waves, and

$$\frac{\partial \tau}{\partial t} + c_2\frac{\partial \tau}{\partial x} - \rho c_2\left(\frac{\partial v}{\partial t} + c_2\frac{\partial v}{\partial x}\right) = \rho c_2^2\frac{\partial u}{\partial y} - c_2\frac{\partial q}{\partial y} \tag{26}$$

$$\frac{\partial \tau}{\partial t} - c_2\frac{\partial \tau}{\partial x} + \rho c_2\left(\frac{\partial v}{\partial t} - c_2\frac{\partial v}{\partial x}\right) = \rho c_2^2\frac{\partial u}{\partial y} + c_2\frac{\partial q}{\partial y} \tag{27}$$

$$\tag{28}$$

which relate to the transverse waves (aka secondary or S-waves). It is easy to write out the four bicharacteristic equations for propagation in the $\pm y$-directions.

3.4 Discussion of Bicharacteristic Discretisations

The numerical use of multidimensional characteristic equations has been attended by continuing disagreement over such matters as which (and even how many) characteristic equations to use, and how to discretize them.

As in the examples above, any characteristic equation is a relationship between interior derivatives in some plane. Ideally the stencil on which it is discretized would comprise only points in that plane. Failing that, the points should lie as close to the plane as possible;
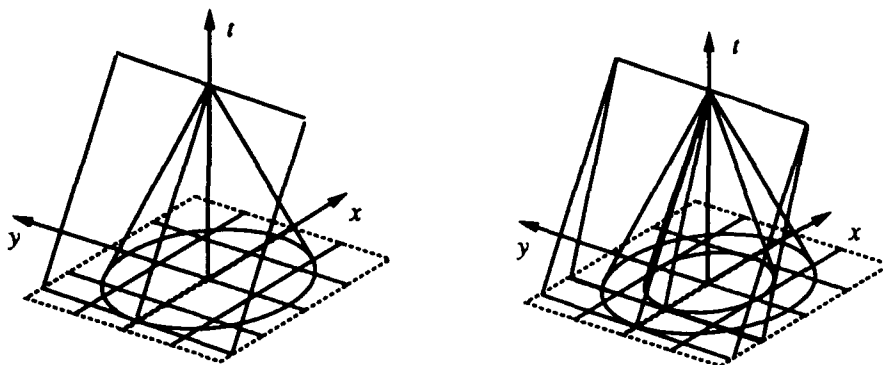
Figure 6: Characteristic planes for waves moving in the positive x-direction, and the characteristic cones. Acoustic problem at left and elastodynamic problem at right.

this lesson can be learned from the one-dimensional case. Bearing this in mind, we consider the issues raised above.

It is sometimes pointed out that although there are infinitely many bicharacteristic equations, corresponding to all possible propagation directions, only a few of these carry independent information. Indeed, since the bicharacteristic equations are merely linear combinations of the given PDEs, it is clear that not more than three of them can be independent for the acoustic problem, or five for the elastodynamic problem. However, this argument applies to the PDEs themselves, acting at a point. The discretized versions should be related to finite regions of space. It makes no algorithmic sense to 'add' the pair of equations (19) and (20) and then discard the terms that apparently 'cancel' because those terms should be evaluated, and in an upwind discretisation are evaluated, at different places. Their difference is what gives the bicharacteristic equations the power to distinguish different kinds of information. On a two-dimensional Cartesian grid there are, for the acoustic and elastodynamic equations respectively, four and eight bicharacteristic equations that can be naturally discretised on compact stencils. All of these carry, in the above sense, independent information, and so ought only to be discretised using points that cluster round the characteristic plane concerned.

The problem then is that there are more bicharacteristic equations than unknowns; four versus three in the acoustic problem, and eight versus five for elastodynamics. This might be called the *counting problem*. In the existing literature it is resolved in one of two ways. One is to consider a reduced number of bicharacteristic equations. For example, in the acoustic problem three bicharacteristics might be considered, spaced at 120°. However, the derivatives in these surfaces then have to be obtained by interpolation, using data that is not the most appropriate. Alternatively, all of the bicharacteristic equations may be employed, but solved in some least-squares sense; again this results in the muddling of information that ought to remain distinct.

The conflict can be resolved, in the present context, by storing the unknowns in a staggered manner. Exactly how this is to be done depends on the way that different variables are coupled in the governing equations, and will be described for specific examples in the next section.
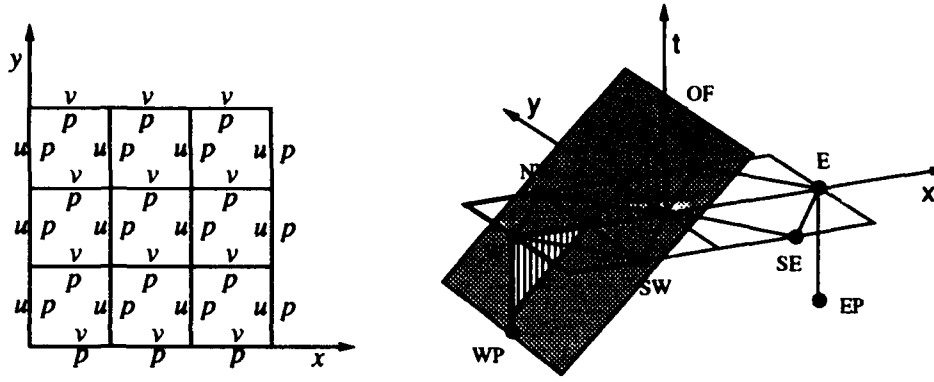
Figure 7: The storage of unknowns on a square grid, and the stencil used to update a u, p point in the second-order scheme. The shaded plane shows a wave moving in the positive x-direction.

4 Staggered Variables

4.1 The Acoustic Problem

Consider the square grid, with uniform spacing h in both directions, shown on the left of Figure 7. The x- and y-velocity components are stored on the mesh lines x, y=constant, as is commonly done for incompressible flows, to achieve compact, centered stencils for all terms. Here, however, pressure is stored at both velocity locations rather than in the cell centers, because the terms that appear in any one bicharacteristic equation must be colocated on an appropriate stencil.

How this is achieved is shown in the right half of the figure. The stencil for the equation describing waves moving in the positive x-direction comprises the points O, NW, SW, and W at time-level n, together with OF at level $n + 1$ and WP at level $n - 1$. At the points OF, O, W and WP the variables u, p are stored. At NW and SW we have v and p. Unique reversible discretizations for (19) and (20) are

$$
\frac{1}{2\Delta t}\left[(p_{OF} - p_O) + \rho a(u_{OF} - u_O)\right] = -\frac{1}{2\Delta t}\left[(p_W - p_{WP}) + \rho a(u_W - u_{WP})\right]
$$
$$
-\frac{a}{h}\left[(p_O - p_W) - \rho a \, \mathrm{div}_{OW})\right]
$$

$$
\frac{1}{2\Delta t}\left[(p_{OF} - p_O) - \rho a(u_{OF} - u_O)\right] = -\frac{1}{2\Delta t}\left[(p_E - p_{EP}) - \rho a(u_E - u_{EP})\right]
$$
$$
+\frac{a}{h}\left[(p_E - p_O) + \rho a \, \mathrm{div}_{EO}\right]
$$

where div_{OW} denotes the 'discrete divergence' $u_O - u_W + v_{NW} - v_{SW}$. This provides two equations for the two unknown values at OF, and eliminates the 'counting problem' previously alluded to. Employing a more concise notation, with δ^+ denoting a forward time difference and δ^- a backward time difference, and defining a Courant number $\nu = (a\Delta t)/h$, this yields update formulae

$$
\delta^+ p_O = -\frac{1}{2}(\delta^- p_W + \delta^- p_E) + \frac{\rho a}{2}(\delta^- u_E - \delta^- u_W)
$$
$$
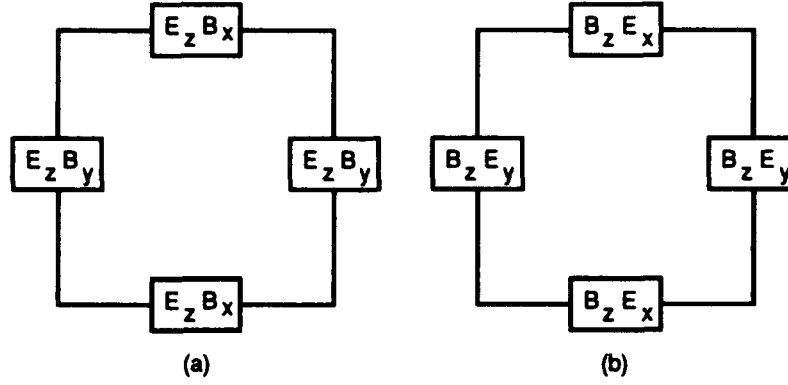+\nu(p_W - 2p_O + p_E - \rho a(\mathrm{div}_{OW} + \mathrm{div}_{EO})) \tag{29}
$$

15

Figure 8: Staggered storage for (a) electrically, and (b) magnetically polarised electromagnetic waves.

$$\delta^+ u_O = -\frac{1}{2}(\delta^- u_W + \delta^- u_E) + \frac{1}{2\rho a}(\delta^- p_E - \delta^- p_W)$$
$$+\nu(\mathrm{div}_{OW} - \mathrm{div}_{EO} + (p_W - p_E)/(\rho a)) \qquad (30)$$

Computing time is saved by storing the terms that appear in the first line of each expression from the previous timestep. The operations that remain are those involved in a first-order upwind scheme, except that the appearance of (div) rather than just $\partial_x u$ imparts an authentically multidimensional flavour.

The scheme is completed by adding a similar update step for the points where v, p are stored.

4.2 Electromagnetics

In two dimensions, this problem has no independent interest, since Maxwell's equations have the same structure as the acoustic equations. All that is needed is to distinguish between the electrically and magnetically polarised cases, for which the respective storage strategies are shown in Figure 8

4.3 Elastodynamics

The storage here follows from the fact that the bicharacteristic equations in the x- and y-directions each contain on their right-hand sides four of the five unknowns, thereby dictating the storage shown in Figure 9. The discretisation is then straightforward.

4.4 Boundary Procedures

Consider any cell of which one edge lies on a boundary. Typically, some even number $2k$ of variables are stored on that edge. To update them, there are k bicharacteristic equations that can be written for the waves that reach the boundary from the cell. These have to be supplemented by k conditions on the boundary itself. In the acoustic example treated below, one boundary is a wall moving in the x-direction in a prescribed manner, so that u is given. The combination $p - \rho a u$ is found from the incoming bicharacteristic, so that p is determined. The velocity v parallel to the wall is not required; in methods with colocated variables some extra condition must be introduced to find it.
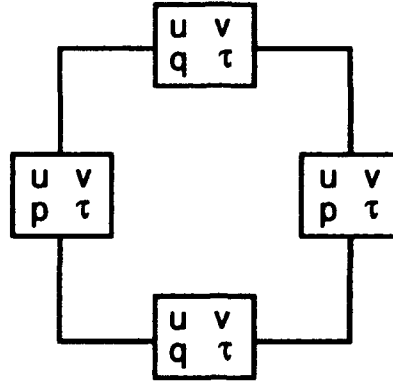
16

Figure 9: Staggered storage for elastodynamic waves.

At open boundaries there are difficulties that go beyond numerical considerations,, since for general wave propagation problems no exact local boundary conditions exist. A crude expedient, adopted in the later examples, is to set to zero, at the boundary, all wavestrengths from outside the boundary. An improved procedure is under investigation.

4.5 Von Neumann Analysis

A von Neumann analysis of the schemes is possible, but complicated by the double storage of unknowns. The acoustic case is presented for illustration, with the values of p that are collocated with v renamed as q. Then one can make the trial solution

$$\begin{pmatrix} p \\ u \\ q \\ v \end{pmatrix} = \Re \begin{pmatrix} \rho a P \\ U \\ \rho a Q \\ V \end{pmatrix} \exp i(n\phi - j\theta_x - k\theta_y),$$

where j, k are counting indices in the x, y-directions. Inserting this into (19) yields

$$(P + U)\left[\sin \frac{\phi}{2} \cos \frac{\phi}{2} \cos \frac{\theta_x}{2} - (\nu - \sin^2 \frac{\phi}{2}) \sin \frac{\theta_x}{2} \right] - V\nu \sin \frac{\theta_y}{2} = 0. \tag{31}$$

Similar relationships can be obtained from the other three equations, and the condition that all four admit a non-trivial solution for P, U, Q, V leads, after a little rearrangement, to the determinant

$$\det \begin{vmatrix} \sin \frac{\phi}{2} \cos \frac{\phi}{2} \cos \frac{\theta_x}{2} & (\nu - \sin^2 \frac{\phi}{2}) \sin \frac{\theta_x}{2} & 0 & \nu \sin \frac{\theta_x}{2} \\ (\nu - \sin^2 \frac{\phi}{2}) \sin \frac{\theta_x}{2} & \sin \frac{\phi}{2} \cos \frac{\phi}{2} \cos \frac{\theta_x}{2} & 0 & 0 \\ 0 & \nu \sin \frac{\theta_y}{2} & \sin \frac{\phi}{2} \cos \frac{\phi}{2} \cos \frac{\theta_y}{2} & (\nu - \sin^2 \frac{\phi}{2}) \sin \frac{\theta_y}{2} \\ 0 & 0 & (\nu - \sin^2 \frac{\phi}{2}) \sin \frac{\theta_y}{2} & \sin \frac{\phi}{2} \cos \frac{\phi}{2} \cos \frac{\theta_y}{2} \end{vmatrix} = 0. \tag{32}$$

This is not very tractable except in the special case $\nu = 1/2$ when the dramatic simplification

$$\cos^2 \phi = \cos^2 \frac{\theta_x}{2} \cos^2 \frac{\theta_y}{2}$$

takes place. We can use this result to study the propagation of a plane inclined wave with $\theta_x = \theta \cos \alpha, \theta_y = \theta \sin \alpha$. We obtain

$$\varepsilon_P = \frac{\phi}{\theta} - \frac{1}{2} \simeq \frac{\theta^2}{192} \sin^2 2\alpha \leq \frac{\pi^2}{48N^2},$$
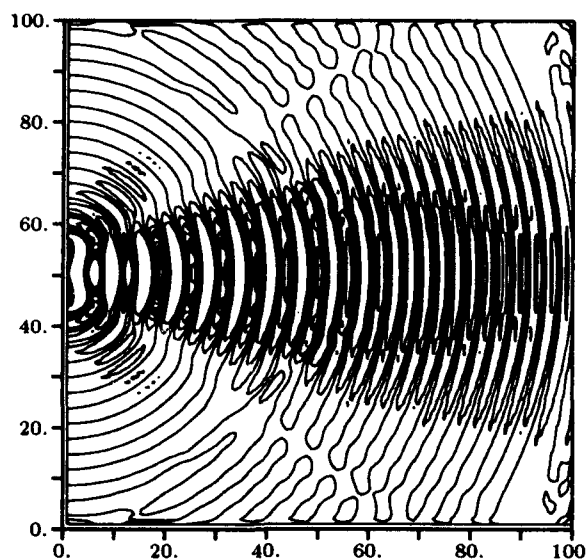
17

Figure 10: Pressure contours due to a wall-mounted oscillating piston.

showing that phase speeds better than 1.0% or 0.1% are achieved for all wave directions with $N \geq 5$ or $N \geq 15$. Thus, the two-dimensional method is isotropic to within the phase error of the one-dimensional method.

5 Numerical Experiments

The first results relate to the acoustic equations solved in axisymmetric coordinates. This requires the addition of a term v/y to the divergence terms in (29,30). The upper, lower, and right boundaries are open. On the left boundary the fluid velocity component u is prescribed. For cell indices 45 through 56 its value at the nth time level is set to

$$u^n = \sin \frac{2\pi\nu n}{N}.$$

Elsewhere it is zero. Thus the boundary conditions simulate an oscillating piston mounted on a plane wall. The parameter N corresponds to the number of mesh points per wavelength. Figure 10 shows a snapshot of pressure contours obtained on a 100×100 grid with $N = 6$ and $\nu = 0.45$.

For this particular problem there is an analytical solution for the envelope of the pressure field on the axis of symmetry [7]. Figure(11) compares this with the numerical prediction on a larger grid (400×400) grid with $N = 8$ and $\nu = 0.45$. It can be seen that the waves travel over 50 wavelengths without any discernable loss of energy. However, careful inspection reveals that the amplitude of the numerical waves is slightly too large in certain regions ($x \simeq 0.15, 0.45, 0.80$). This is due the numerical wavespeed being slightly anisotropic. Waves that reach the same place by different routes are therefore slighly out of phase, and their mutual interference is not correct. Solutions computed woth $N = 4$ (not shown) exhibit pronounced spurious interference patterns.
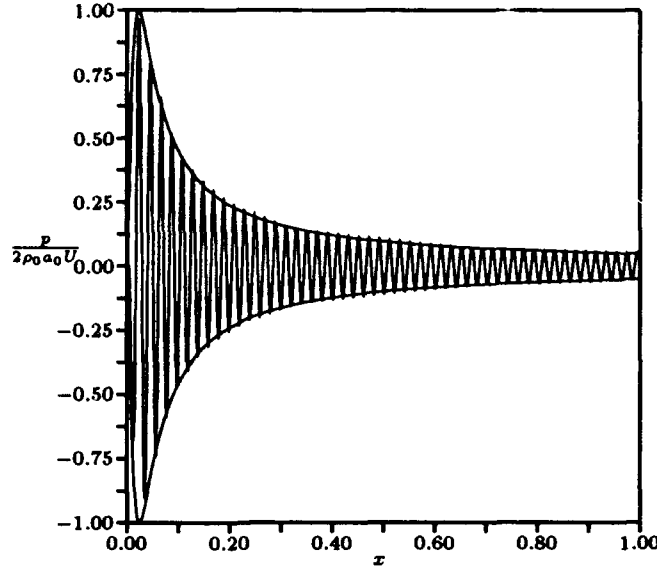
18

Figure 11: Pressure distribution on the axis of symmetry due to a wall-mounted oscillating piston.

The second test problem is from elastodynamics. The upper boundary is a free surface, on which $q = \tau = 0$, except at a single point (upper left corner) where q is specified as a point loading;

$$ q(t) = -\frac{4}{\sigma^2}(t - t_s) \left[\exp -2 \left(\frac{t - t_s}{\sigma} \right)^2 - \exp -2 \left(\frac{t_s}{\sigma} \right)^2 \right]. $$

This loading is taken from [8], and simulates a positive impulsive load, followed by a negative impulsive load. The case with truly impulsive loading is called Lamb's problem. The left boundary is a plane of symmetry, and the right and lower boundaries are open. This is harder than the acoustic problem because of the two different wavespeeds. The slower S-waves (transverse waves) have a shorter spatial wavelength and so the mesh requirement is driven by the need to resolve them. The faster P-waves (longitudinal waves) then have about twice as many points per wavelength as they would require by themselves.

Figure 12 shows the various waves that are generated, through contours of the quantity $p + q$. The mesh size is 200 × 200, which resolves the S-wave over about 10 points, and the P-wave over about 20. The head wave is an S-wave generated by interaction of the P-wave with the surface, and the Rayleigh wave is a feature that stays close to the surface and travels slightly slower than the S-wave. In this simulation, it has not yet detached itself from the S-wave. More discussion of Lamb's problem, including an analytical solution of the impulsive loading case, can be found in texts on elastodynamics, such as [9].

6 Three-dimensional Applications

The method applies naturally in three dimensions; the correct storage strategies are easily determined. In various cases, the quantities stored on a face $x = const$ are; for acoustics (u, p), for electromagnetics (B_y, B_z, E_y, E_z), and for elastodynamics $(u, v, w, \sigma_{xx}, \sigma_{xy}, \sigma_{xz})$.
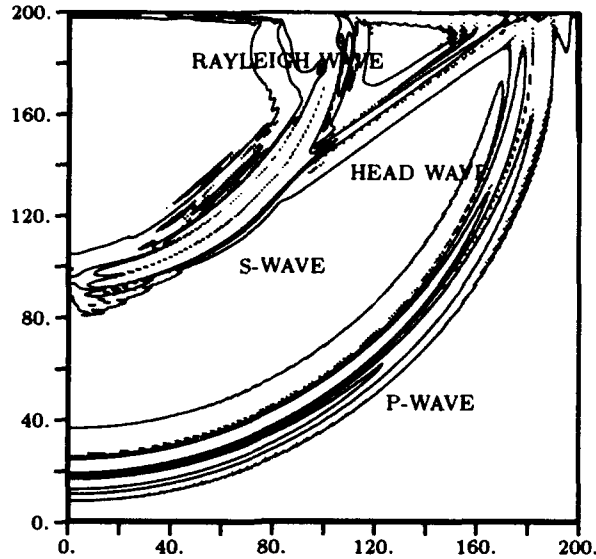
Figure 12: Contours of the sum of normal stresses for a smoothed version of Lamb's problem.

Calculations of three-dimensional electromagnetic problems have been presented by Nguyen and Roe [10].

A central leapfrog scheme due to Yee [11] has been popular in electromagnetics, which also uses staggered storage. The strategy in that scheme is motivated by the wish to achieve a compact discretisation for each component of the curl operator, centered where it must be used to create a time derivative. On a cubical array, the center of each face contains the normal component of the magnetic field, and the center of each edge contains the parallel component of the electric field. Accounting for the way that edges and faces are shared reveals that each cube is the site of six pieces of information. The present scheme stores twelve. This is outweighed by the ability of the present scheme to take larger timesteps (by a factor $D^{\frac{1}{2}}$, where D is the number of space dimensions), and to work with coarser grids (by a factor 2^D). These are the gains and losses of the characteristic formulation. However, a complete comparison remains to be done.

7 Conclusions and Future Work

Building on the one-dimensional foundations laid in [1], we have presented a new type of algorithm for linear wave propagation. The extension to higher dimensions requires the resolution of a counting problem common to many numerical exploitations of the bicharacteristic equations. This is done here by adopting a particular form of staggered storage.

Future publications will document the application of the method to very long-time computations in the presence of source terms, and on dynamically adaptive grids.

20

8 References

1. A. ISERLES, Generalised leapfrog schemes, *IMA Jnl Num. Anal.* vol 6, 1986.

2. L.N. TRETETHEN, Group velocity in finite-difference schemes, *SIAM Review* vol 24, 1982, pp 113-136.

3. J. P. THOMAS, P.L. ROE, Development of non-dissipative numerical schemes for computational aeroacoustics, AIAA paper 93-3382-CP, Orlando, 1993, AIAA CP 933, 1993.

4. P. I. CHUSKIN, Numerical methods of characteristics for three-dimensional supersonic flows, *Progress in Aeronautical Sciences*, vol 9, Pergammon, 1968.

5. R. CAMERARO, Numerical Solution of Internal and External Flows at High Incidence, PhD Thesis, McGill University, 1973.

6. I. H. PARPIA, C. P. KENTZER, M. H. WILLIAMS, Multidimensional time-dependent method of characteristics, *Computers and Fluids* vol 16, 1988.

7. L.E. KINSLER, A.B. COPPENS, A.R. FREY, J.V. SANDERS, *Fundamentals of Acoustics*, John Wiley, 1982.

8. A. BAYLISS, K.E. JORDAN, B.J. LEMESURIER, E. TURKEL, A fourth-order accurate finite-difference scheme for the computation of elastic waves, *Bull. Seismological Soc. Amer.*, **76**, 4, p 115, 1986.

9. J.A. HUDSON, *The Excitation and Propagation of Elastic Waves*, Cambridge, 1980

10. B. NGUYEN, P.L. ROE,, Application of an upwind leapfrog method for electromagnetics, in *10th Annual Review of Progress in Applied Computational Electromagnetics*, vol 1, pp 446-458, 1994.

11. K. YEE, Numerical solution of initial-boundary value problems involving Maxwell's equations in isotropic media, IEEE Transactions on Antennae and Propagation, AP-16, (1966), pp302-307.

REPORT DOCUMENTATION PAGE

1. AGENCY USE ONLY*(Leave blank)*	2. REPORT DATE July 1994	3. REPORT TYPE AND DATES COVERED Contractor Report

4. TITLE AND SUBTITLE LINEAR BICHARACTERISTIC SCHEMES WITHOUT DISSIPATION	5. FUNDING NUMBERS C NAS1-19480 WU 505-90-52-01
6. AUTHOR(S) Philip Roe	

7. PERFORMING ORGANIZATION NAME(S) AND ADDRESS(ES) Institute for Computer Applications in Science and Engineering Mail Stop 132C, NASA Langley Research Center Hampton, VA 23681-0001	8. PERFORMING ORGANIZATION REPORT NUMBER ICASE Report No. 94-65

9. SPONSORING/MONITORING AGENCY NAME(S) AND ADDRESS(ES) National Aeronautics and Space Administration Langley Research Center Hampton, VA 23681-0001	10. SPONSORING/MONITORING AGENCY REPORT NUMBER NASA CR-194957 ICASE Report No. 94-65

11. SUPPLEMENTARY NOTES

12a. DISTRIBUTION/AVAILABILITY STATEMENT Unclassified–Unlimited Subject Category 64	12b. DISTRIBUTION CODE

13. ABSTRACT *(Maximum 200 words)*

This paper is concerned with developing methods for the propagation of linear waves in several space dimensions. The methods are time-reversible, and hence free from numerical dissipation. They are based on bicharacteristic forms of the governing equations, and are made possible by adopting forms of staggered storage that depend on the precise equations under consideration. Analysis is presented for the equations of acoustics, electromagnetics, and elastodynamics.

14. SUBJECT TERMS wave equations, bicharacteristic methods, numerical dissipation	15. NUMBER OF PAGES 23
	16. PRICE CODE A03

17. SECURITY CLASSIFICATION OF REPORT Unclassified	18. SECURITY CLASSIFICATION OF THIS PAGE Unclassified	19. SECURITY CLASSIFICATION OF ABSTRACT	20. LIMITATION OF ABSTRACT